Detection of AMSR-E Radio Frequency Interference over Ocean

X. Tian[1], Z. Qin[1], X. Zou[1], and F. Weng[2]

[1] Department of Earth, Ocean and Atmospheric Sciences, Florida State University, USA

[2] National Environmental Satellite, Data & Information Service, National Oceanic and Atmospheric Administration, Washington, D. C., USA

Abstract

The geostationary satellite television (TV) signals that are reflected off the ocean surfaces could enter the satellite microwave imager antenna's field-of-views (FOVs), resulting in Radio Frequency Interference (RFI) contamination in Advanced Microwave Scanning Radiometer – EOS (AMSR-E) 10.65 and 18.7 GHz channels. If not detected, the presence of RFI signals can result in erroneous retrievals of oceanic environmental parameters (e.g., sea surface temperature, sea surface wind speed, rain water path) from microwave imaging radiance measurements. In this study, a normalized Principal Component Analysis (NPCA) method is proposed for RFI detection of AMSR-E observations over ocean. It is found that the RFI-contaminated observations on AMSR-E descending nodes at 10.65 and 18.7 GHz can be effectively detected near coastal areas surrounding Europe and North America continents. The proposed NPCA algorithm is applicable in an operational environment for fast data processing and data dissemination, and is different from earlier methods, which often require a priori information.

Introduction

The AMSR-E is a conically scanning microwave imager on board EOS-Aqua satellite, which was successfully launched into a polar-orbit in May 2002 with an equator-crossing time (ECT) at 1:30pm. The AMSR-E measurements at 6.925GHz (C-band), 10.65GHz (X-band) and 18.7 GHz (K-band) are mainly used for retrieving the environmental parameters over oceans and land. However, these low microwave frequencies of AMSR-E operate in unprotected frequency bands. Both the AMSR-E X-band and K-band channels are used in satellite communications. However, measurements of natural oceanic thermal emission at AMSR-E channel frequencies could be interfered by the geostationary satellite television (TV) signals reflected off the ocean surfaces. At microwave frequencies, the ocean surface has much larger reflectance than land surface due to the high permittivity value of seawater. Such a phenomenon of satellite-measured passive microwave thermal emission being mixed with the TV signals emanating from geostationary satellites (e.g., Astra, Hotbird, Atlantic Bird 4A, DirecTV-10/11 etc.) and reflected off the ocean surfaces is referred to as ocean Radio-Frequency Interference (RFI). A schematic illustration of an oceanic RFI is provided in Fig. 1. With the expanding demand for fixed-satellite service (FSS) technology, increasing amounts of RFI are now affecting oceanic measurements from satellite passive microwave instruments.

The RFI-contaminated brightness temperature measurements, if not identified and excluded in the algorithms, would introduce appreciable errors in the AMSR-E retrievals of precipitable water (PW), sea surface wind (SSW), and sea surface temperature (SST) variables. It is therefore important to develop effective algorithms to detect RFI contaminated data prior to carrying out AMSR-E product retrieval and data assimilation.

Microwave emissivity over oceans is much lower than that over land. The cloud and precipitation can increase the thermal emission and therefore significantly increase the brightness temperature at lower frequencies. Such an increase in AMSR-E measured brightness temperatures could be of similar magnitude to an increase introduced by RFI associated with TV signal reflection from the ocean surface. It is therefore extremely challenging to develop a robust technique for detecting the oceanic RFI signals so that the weather signals do not appear as "false" RFI signals. There are two methods that were employed for identifying RFI signatures over oceans: a Chi-square probability method and a regression method. The Chi-square method looks for RFI occurrence that isn't geophysically explainable. In Chi-square probability algorithm, an RFI detection method is developed using a time-averaged statistical quantity based on a fact that the source of the oceanic RFI, TV signals, are fixed in location and time, while weather signals associated with cloud and precipitation are transient. The goodness-of-fit (i.e., Chi-square probability) is used for RFI detection. The lower the goodness-of-fit is, the higher the probability of the presence of RFI is expected. In Li et al (2006), a regression model is first established to predict RFI-free brightness temperatures at X- and K-bands from the other WindSat channels. The difference between WindSat oceanic observations and regression-model-predicted brightness temperatures is then used for oceanic RFI detection. The larger the difference, the stronger the RFI intensity is likely to be.

In this study, a PCA-based method is developed to detect the RFI signals in AMSR-E data over the global oceans. Compared to the above-mentioned two prior methods, this new PCA-based method has the following two outstanding features: (i) it involves only observations; and (ii) it can be applied at the granule data level. There is no need for training data, a priori determination of rain-free and RFI-free data, and satellite retrieval.

AMSR-E Data Description

AMSR-E is one of the six instruments on board the NASA Aqua satellite. Aqua satellite was launched into a sun-synchronous orbit at an altitude of 705 km with a swath width of 1445 km. The equator crossing time (ECT) of its ascending node is 1:30pm. AMSR-E is a twelve-channel, six-frequency, total power passive-microwave conical-scanning radiometer system. The Earth-emitted microwave radiation entering the antenna beams that view the Earth at an incidence angle of 55o is collected. It measures vertically and horizontally polarized brightness temperatures at 6.925, 10.65, 18.7, 23.8, 36.5, and 89.0 GHz. The across-track and along-track spatial resolutions of the individual ground instantaneous field-of-view (IFOV) measurements are 75 x 43 km at 6.925 GHz, 51 x 29 km at 10.65 GHz, 27 x 16 km at 18.7 GHz, 32 x 18 km at 23.8 GHz, 14 x 8 km at 36.5 GHz and 6 x 4 km at 89.0 GHz, respectively. The sampling interval is 10 km for 6-36 GHz channels and 5 km for the 89 GHz channel.

AMSR-E is the heritage of Scanning Multichannel Microwave Radiometer (SMMR) on board Nimbus 7 and Seasat, Special Sensor Microwave Imager (SSM/I) on board the Defense Meteorological Satellite Program (DMSP), and Advanced Microwave Scanning Radiometer (AMSR) on board the Advanced Earth Observing Satellite II (ADEOS II). It is worth mentioning that the successor of AMSR-E is AMSR-2, which was on board the Global Change Observation Mission 1st – Water (GCOM-W1) satellite launched on May 18, 2012. The mission of AMSR-2 is similar to that of AMSR-E except for two additional new channels located at 7.3 GHz, which is adjacent to 6.925 GHz, for the purpose of RFI mitigation over land.

Center Frequency		Band Width		Polarization		Spatial Resolution		Sampling Interval	
GHz		MHz				km		AMSR-E	AMSR2
AMSR-E	AMSR2	AMSR-E	AMSR2	AMSR-E	AMSR2	AMSR-E	AMSR2		
6.925	6.925/7.3	350				43x75	35x62		
10.65		351				29x51	24x42		
18.7		352				16x27	14x22		
23.8		353		V/H		18x32	15x26	10	
36.5		354				8x14	7x12		
89		355				4x6	3x5	5	

Schematic Illustration of RFI

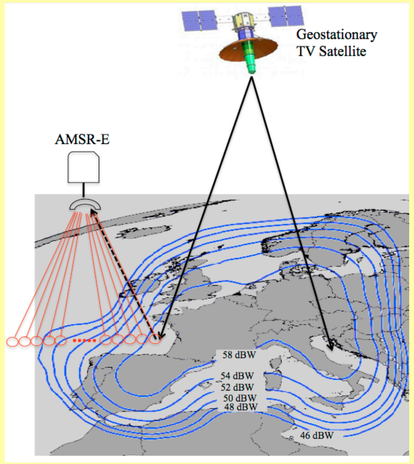

Fig. 1: A schematic illustration of RFI of AMSR-E earth views (red) with TV signals reflected off from ocean surfaces (black dashed). Satellite downlink beam coverage is shown in blue curves, which are obtained from http://www.satsig.net/tooway/tooway-ka-band-downlink-hotbird.gif.

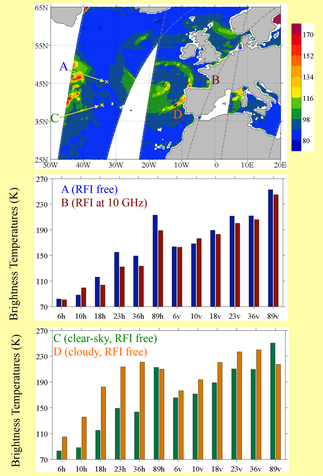

Fig. 2: (a) Spatial distribution of brightness temperatures at 10 GHz horizontal polarization channel on February 16, 2011 over ocean around Europe. (b) Brightness temperatures of all AMSR-E channels at four arbitrarily chosen data points A (blue), B (red), C (green) and D (orange) on February 16, 2011. The geographic locations of points A-D are indicated in Fig. 2a.

DPCA Methodology

$$\vec{V}_i = \begin{pmatrix} \frac{T^o_{b,6h}-\mu}{\sigma} \\ \frac{T^o_{b,6v}-\mu}{\sigma} \\ \vdots \\ \frac{T^o_{b,89h}-\mu}{\sigma} \\ \frac{T^o_{b,89v}-\mu}{\sigma} \end{pmatrix}_i = \begin{pmatrix} T_{b,6h} \\ T_{b,6v} \\ \vdots \\ T_{b,89h} \\ T_{b,89v} \end{pmatrix}_i$$

$$\vec{R}_{10,h,i} = \begin{pmatrix} T_{b,10h}-T_{b,18h} \\ T_{b,18h}-T_{b,23h} \\ T_{b,18v}-T_{b,23v} \\ T_{b,23h}-T_{b,36h} \\ T_{b,23v}-T_{b,36v} \end{pmatrix}_i \quad \vec{R}_{10v,i} = \begin{pmatrix} T_{b,10v}-T_{b,18v} \\ T_{b,18h}-T_{b,23h} \\ T_{b,18v}-T_{b,23v} \\ T_{b,23h}-T_{b,36h} \\ T_{b,23v}-T_{b,36v} \end{pmatrix}_i \quad \vec{R}_{18h,i} = \begin{pmatrix} T_{b,18h}-T_{b,23h} \\ T_{b,23h}-T_{b,36h} \\ T_{b,23v}-T_{b,36v} \\ T_{b,36h}-T_{b,89h} \\ T_{b,36v}-T_{b,89v} \end{pmatrix}_i \quad \vec{R}_{18v,i} = \begin{pmatrix} T_{b,18v}-T_{b,23v} \\ T_{b,23h}-T_{b,36h} \\ T_{b,23v}-T_{b,36v} \\ T_{b,36h}-T_{b,89h} \\ T_{b,36v}-T_{b,89v} \end{pmatrix}_i$$

The data matrix, **A**, can be reconstructed as

$\mathbf{A} = \sum_{i=1}^{5} \vec{e}_i \vec{u}_i$, in which $\mathbf{A}_i = \vec{e}_i \vec{u}_i$ is the component in **A** that accounts for the ith greatest variance. The first component in A3, corresponding to the targeted spectral difference, will be referred to as the indicator of how strong RFI is, calculated as (e.g., 10.65 GHz H-Pol case)

$$RI_i = \sigma_i \bullet \left(T^{4_i}_{b,10h} - T^{4_i}_{b,18h}\right)$$

$$\begin{pmatrix} \vec{u}_1 \\ \vec{u}_2 \\ \vdots \\ \vec{u}_5 \end{pmatrix} = \mathbf{E}^T \mathbf{A} \qquad \vec{u}_i = \begin{bmatrix} u_{i,1} & u_{i,2} & \cdots & u_{i,5} \end{bmatrix}$$

$$\mathbf{A}_{5\times N} = \begin{pmatrix} \vec{R}_{xx,1} & \vec{R}_{xx,2} & \cdots & \vec{R}_{xx,N} \end{pmatrix}$$ Where "*xx*" can be any of the four channel cases above

$$\mathbf{R}_{5\times 5} = \mathbf{A}\mathbf{A}^T$$

$\mathbf{R}\vec{e}_i = \lambda_i \vec{e}_i$ or $\mathbf{R} = \mathbf{E}\Lambda\mathbf{E}^T$

Where $\Lambda = \begin{pmatrix} \lambda_1 & \cdots & 0 \\ \vdots & \ddots & \vdots \\ 0 & \cdots & \lambda_5 \end{pmatrix}$, $\mathbf{E} = \begin{bmatrix} \vec{e}_1, & \vec{e}_2, & \cdots & \vec{e}_5 \end{bmatrix}$

RFI Intensities

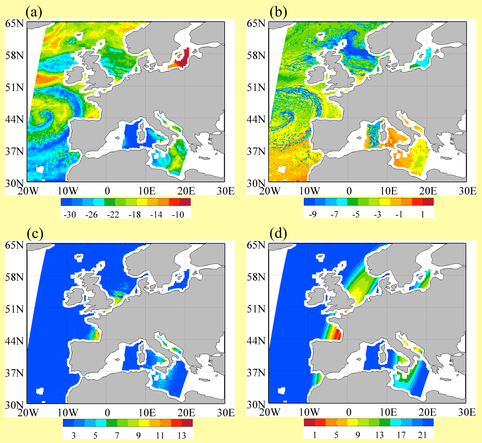

Fig. 3: Spectral differences between 10.65 GHz horizontally polarized channel and that of 18.7 GHz corresponding to the data matrices (a) , (b) , and (c) (RFI signal intensity) found by the NPCA method for observations on February 16, 2011. (d) Satellite glint angle.

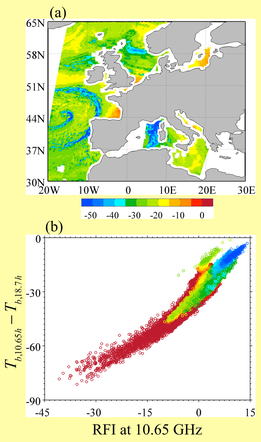

Fig. 4: (a) Spectral differences between 10.65 and 18.7 GHz horizontal polarization (i.e.,) on February 16, 2011, and (b) scatter plot between RFI intensities shown in Fig. 3c and the spectral differences shown in (a).

RFI Detection at 10.65 GHz

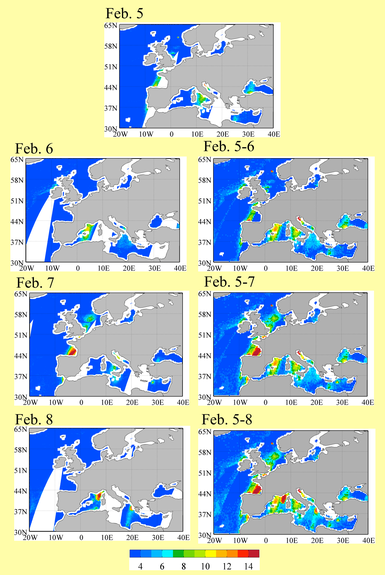

Fig. 5: Daily (left panels) and accumulative (right panels) RFI intensity maps at 10.65 GHz horizontal polarization from 5-8 February 2011 around Europe.

RFI Detection at 18.7 GHz

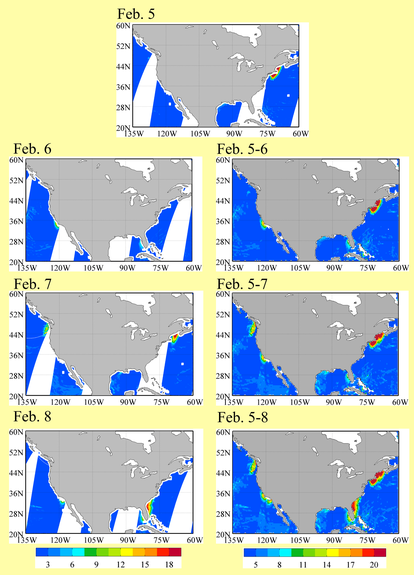

Fig. 6: Daily (left panels) and accumulative (right panels) RFI intensity maps at 18.7 GHz horizontal polarization from 5-8 February 2011 around United States.

Monthly Mean of Detected RFI Signatures

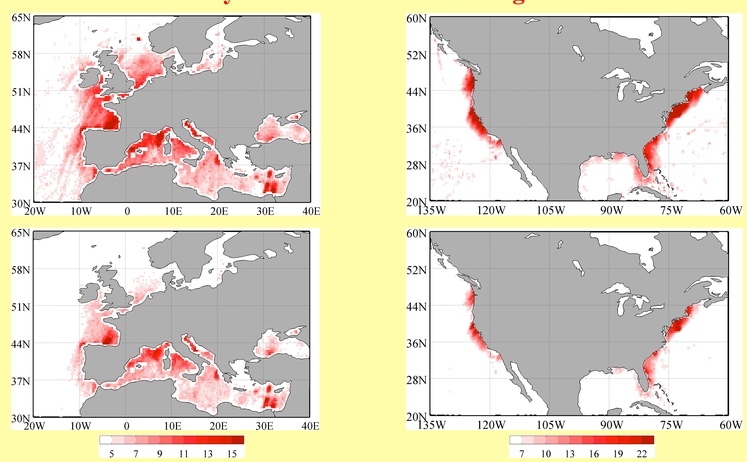

Fig. 7: Monthly average RFI intensity maps for AMSR-E (a)-(b) 10.65 GHz and (c)-(d) 18.7 GHz channels at horizontal (upper panels) and vertical polarization (lower panels) for all descending portions of AMSR-E orbits from February 1 to 18, 2011.

Summary and Conclusions

RFI detection for satellite low-frequency microwave imager radiances over oceans is important and challenging. The RFI contaminations must be reliably identified before these data can be used for either geophysical retrievals or data assimilation in numerical weather prediction models. In this paper, examinations are performed on the geometric relationship between reflected TV signals, the source of RFI, and AMSR-E observations. Then the results of a NPCA method for detecting RFI signals in AMSR-E data over oceans are presented.

By calculating the angles between the AMSR-E observation beam vector and the vector of reflected TV signal from geostationary TV satellites, it is convincing that the likely source of the oceanic RFI comes from the broadcasting signals from European geostationary television (TV) satellites above the equator. The NPCA method takes into account the multi-channel correlation for natural ocean surface radiations, as well as the de-correlation channels at different frequencies in the presence of RFI signals. The methodologies developed in this paper characterized by the presence of small-scale weather such as clouds and precipitation that could cause false alarms during detection are applied to RFI identification of AMSR-E data over oceans. A strong RFI is visible for X and K-band channels at both horizontal and vertical polarization over oceans near coastal regions. Consistent with the cause of the ocean RFI signals, measurements of the natural thermal emission from the AMSR-E instrument over oceans are interfered with by the geostationary satellite television (TV) signals reflected off the ocean surfaces. Strong RFI signals are populated along the east, south and west coastal areas of the United States in the AMSR-E K-band data in descending nodes. There are also very strong oceanic RFI signals in the AMSR-E X-band data in the Mediterranean Sea, the Adriatic Sea north of Italy, and around Sicily. The RFI locations are also quite persistent for every AMSR-E descending swath passing over these regions with similar observation geometry.

The NPCA works at any geographical location over global oceans in all weather conditions. Being applicable at the granule data level, it offers an operationally feasible global RFI detection method for AMSR-E data at X- and K-bands.

Zou, X., J. Zhao, F. Weng and Z. Qin, 2012: Detection of Radio-Frequency Interference Signal Over Land From FY-3B Microwave Radiation Imager (MWRI), *IEEE Trans. Geosci. Remote Sens.*, **50**, pp. 4994-5003, doi: 10.1109/TGRS.2012.2191792.

Zhao, J., X. Zou, and F. Weng, 2013: WindSat Radio-Frequency Interference Signature and Its Identification Over Greenland and Antarctic, *IEEE Trans. Geosci. Remote Sens.*, **51**, pp. 4830-4839, doi: 10.1109/TGRS.2012.2230634.